Clinical Neurophysiology 130 (2019) 1–11

Contents lists available at ScienceDirect

Clinical Neurophysiology

journal homepage: www.elsevier.com/locate/clinph

Visualization of the electrical activity of the cauda equina using a magnetospinography system in healthy subjects

Shuta Ushio [a], Yuko Hoshino [b], Shigenori Kawabata [a,b,*], Yoshiaki Adachi [c], Kensuke Sekihara [b], Satoshi Sumiya [a], Dai Ukegawa [a], Kyohei Sakaki [a], Taishi Watanabe [a,d], Yuki Hasegawa [b], Atsushi Okawa [a]

[a] Department of Orthopedic Surgery, Tokyo Medical and Dental University, 1-5-45 Yushima, Bunkyo-ku, Tokyo 113-8510, Japan
[b] Department of Advanced Technology in Medicine, Graduate School of Tokyo Medical and Dental University, 1-5-45 Yushima, Bunkyo-ku, Tokyo 113-8510, Japan
[c] Applied Electronics Laboratory, Kanazawa Institute of Technology, Kanazawa-shi, Ishikawa 920-1331, Japan
[d] RICOH Company, Ltd., 16-1 Shinei-cho, Tsuzuki-ku, Yokohama, Kanagawa 224-0035, Japan

ARTICLE INFO

Article history:
Accepted 2 November 2018
Available online 12 November 2018

Keywords:
Magnetospinography
Visualization of neural activity
Cauda equina
Conduction velocity
Evoked magnetic field
Peroneal nerve

HIGHLIGHTS

- Magnetospinography visualized the electrical activity in the cauda equina.
- The conduction velocities were obtained from reconstructed currents in the cauda equina.
- Magnetospinography is expected to become a noninvasive functional examination technique for lumbar disease.

ABSTRACT

Objective: To establish a method to measure cauda equina action fields (CEAFs) and visualize the electrical activities of the cauda equina in a broadly aged group of healthy adults.
Methods: Using a 124-channel magnetospinography (MSG) system with superconducting interference devices, the CEAFs of 43 healthy volunteers (22–64 years of age) were measured after stimulation of the peroneal nerve at the knee. Reconstructed currents were obtained from the CEAFs and superimposed on the X-ray image. Conduction velocities were also calculated from the waveform of the reconstructed currents.
Results: The reconstructed currents were successfully visualized. They flowed into the L5/S1 foramen about 8.25–8.95 ms after the stimulation and propagated cranially along the spinal canal. In 32 subjects (74%), the conduction velocities of the reconstructed currents in the cauda equina could be calculated from the peak latency at the L2–L5 level.
Conclusions: MSG visualized the electrical activity of the cauda equina after peroneal nerve stimulation in healthy adults. In addition, the conduction velocities of the reconstructed currents in the cauda equina could be calculated, despite previously being difficult to measure.
Significance: MSG has the potential to be a novel and noninvasive functional examination for lumbar spinal disease.

1. Introduction

In lumbar spinal diseases such as lumbar spinal canal stenosis, compression lesions in multiple vertebrae are often found in imaging examinations. However, it is often difficult to evaluate the true lesion sites responsible for symptoms by imaging techniques alone (Kent et al., 1992; Mamisch et al., 2012). In addition, it is often necessary to evaluate the locations of the spinal nerve compression, such as intra-canal, intra-foraminal, or extra-foraminal, to choose the appropriate surgical technique (Macnab, 1971; Wiltse et al., 1984; Kunogi and Hasue, 1991; Olsewski et al., 1991). Therefore, functional examinations such as electrophysiological diagnostic

Abbreviations: CEAF, cauda equina action field; CEAP, cauda equina action potential; CECT, cauda equina conduction time; CV, conduction velocity; DSSP, dual signal subspace projection; MSG, magnetospinography; SEP, somatosensory evoked potential; SN, signal-to-noise; SNAP, sensory nerve action potential; SQUID, superconducting quantum interference device; UGRENS, unit gain constraint recursively applied null-steering spatial filtering.

* Corresponding author at: Department of Advanced Technology in Medicine, Graduated School of Tokyo Medical and Dental University, 1-5-45 Yushima, Bunkyo-ku, Tokyo 113-8510, Japan.
E-mail addresses: ushio.orth@tmd.ac.jp (S. Ushio), hoshino.atm@tmd.ac.jp (Y. Hoshino), kawabata.orth@tmd.ac.jp (S. Kawabata), k-sekihara@nifty.com (K. Sekihara), d_ukegawa.orth@tmd.ac.jp (D. Ukegawa), okawa.orth@tmd.ac.jp (A. Okawa).

https://doi.org/10.1016/j.clinph.2018.11.001
1388-2457/

methods are important to determine the indications for surgical treatment and the appropriate operation.

However, it is difficult to measure the electrical neural activity of the cauda equina because the electric potential is affected by the surrounding tissues, including the cerebrospinal fluid. For the same reason, accurate recording of the electric potentials of the lumbar nerve root from the body surface is also difficult. In addition, the cauda equina consists of several spinal nerves, complicating the evaluation of individual neural activities. Some physiological or electrophysiological modalities have been used to determine lesion sites, such as spinal nerve block, somatosensory evoked potential (SEP), sensory nerve action potential (SNAP), cauda equina action potentials (CEAPs), and cauda equina conduction time (CECT). Despite their utility, they also have some disadvantages. For example, the spinal nerve block procedure induces intense pain (Jonsson et al., 1988; Yeom et al., 2008), and SEP is often unable to provide accurate information, including conduction velocity (CV) (Cracco, 1973; Kakigi et al., 1982; Yamada et al., 1982). Although SNAP can detect lesions in distal spinal nerves, it is absent in some normal subjects (Levin, 1998; Ando et al., 2013). Because CEAPs are intraoperatively recorded from the ligamentum flavum (Taniguchi et al., 2005), it cannot be used as a preoperative examination. Additionally, because CECT represents the conduction time of the sum of neural activities in the cauda equine, the function of spinal nerves cannot be evaluated (Matsumoto et al., 2009; Senocak et al., 2009; Secil et al., 2012; Imajo et al., 2017). Therefore, a noninvasive functional examination method with better temporal and spatial resolution is desired.

Because the magnetic field itself is hardly affected by the surrounding tissue, it has theoretically high spatial resolution compared with electric potential recording (Trahms et al., 1989; Hashimoto et al., 1991). Therefore, it has the possibility to be a reliable examination method for the diagnosis of lesion sites in deep nerves, such as the spinal cord and cauda equina.

When a nerve is electrically stimulated, transmembrane ionic currents arise at a depolarization site in the nerve. Accordingly, intra-axonal currents and volume currents are derived from the voltage difference between the depolarization site and the circumferential tissue (Fig. 1). Here, we defined volume currents as all currents in the volume conductor flowing into the depolarization site and flowing out from the nerve. These intra-axonal currents and volume currents generate magnetic fields based on the Biot-Savart law. Green arrows in Fig. 1 indicate magnetic fields resulting from intra-axonal currents (magnetic fields from volume currents are not depicted). Although the induced biomagnetic signal is very small, with a magnitude about 10^{-9} that of geomagnetism (Wijesinghe, 2010), it can be recorded with a highly sensitive magnetic field sensor installed in a magnetically shielded room.

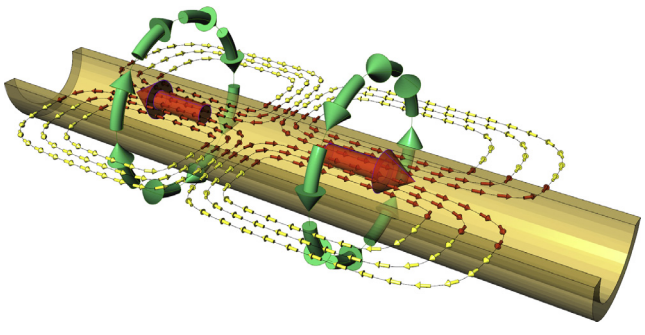

Fig. 1. Schematic illustration of intra-axonal currents (red arrows), volume currents (yellow arrows flowing into the depolarization site and flowing out of the nerve), and magnetic fields (green arrows) resulting from intra-axonal currents (magnetic fields generated by volume currents are not illustrated here). This figure was modified from original version in a report by Sumiya et al. (DOI: https://doi.org//10.1038/s41598-017-02406-8) under CC-BY 4.0.

Our group has developed a magnetospinography (MSG) system using superconducting quantum interference device (SQUID) sensors. Each sensor can detect three directional magnetic field components. By arranging the SQUID sensors, it is possible to simultaneously scan a wide area and to create a contour map of the recorded magnetic field. We have also developed a signal processing method to visualize neural current sources reconstructed from the recorded magnetic field. In addition, the reconstructed current map enables a more detailed evaluation of neural electrical activity.

We previously reported on the diagnosis of compressive spinal cord injury by measurement of evoked magnetic fields in animals (Kawabata et al., 2002; Ohkubo et al., 2003; Tomori et al., 2010). We also closely evaluated magnetic fields of injured nerves using isolated peripheral nerves of rabbits (Fukuoka et al., 2002, 2004) and recorded the magnetic fields of the cervical spinal cord of healthy subjects (Sumiya et al., 2017). We have also recorded evoked magnetic fields from the lumbar region in response to electrical stimulation in the lower extremities in both animals and humans (Tomizawa et al., 2008; Ishii et al., 2012). These studies showed that MSG has the possibility to be a beneficial functional examination for the spinal cord and cauda equina. However, there are still some points to be considered. For example, Ishii et al. (2012) recorded evoked magnetic fields from the lumbar region generated by electrical stimulation of the tibial nerves in healthy subjects in their 20s and 30s. However, the older the subject, the lower the lumbar curve and the poorer the fit of the recording system. Because the magnitude of the magnetic field is inversely proportional to the square of the distance, this misalignment decreased the recorded magnetic fields. Furthermore, when the tibial nerve was electrically stimulated at a region closer to the measurement area to obtain a larger evoked magnetic field, the stimulation artifacts concurrently became larger.

In this study, we used a newly developed MSG system with a measurement area that is wider and has an improved curved shape. We also used a newly devised artifact removal method. The purpose of this study was to establish a method to measure weak cauda equina action fields (CEAFs) from the body surface and to visualize the electrical activities of the cauda equina. Here, we defined action fields as the magnetic fields generated by the electrical activity of the nerve.

2. Methods

2.1. MSG system

Our newly developed 124-channel SQUID biomagnetometer system (Adachi et al., 2015) has a wider sensor area and a more suitable curvature for lumbar lordosis as compared with the former system (Adachi et al., 2007, 2009, 2011, 2013) (Fig. 2). Briefly, the system has 40 vector-type SQUID gradiometers and four axial-type gradiometers arranged in an area of 180 mm × 130 mm along the cylindrical surface with a radius of 200 mm, as shown in Fig. 2. The sensors in the four corners (gray circles in Fig. 2a) are axial-type gradiometers and detect magnetic fields in the Z direction. The data from these four sensors were also used for acquiring positional information. All of the other 40 sensors (white circles in Fig. 2a) have two planar-type gradiometers and one axial-type gradiometer placed orthogonally to each other to simultaneously detect magnetic fields in three directions. The baseline length of each gradiometric pickup coil was 68 mm and the noise level was typically less than 4 $fT/Hz^{0.5}$ in the white region. The X direction was assumed to be the direction from the left to the right of

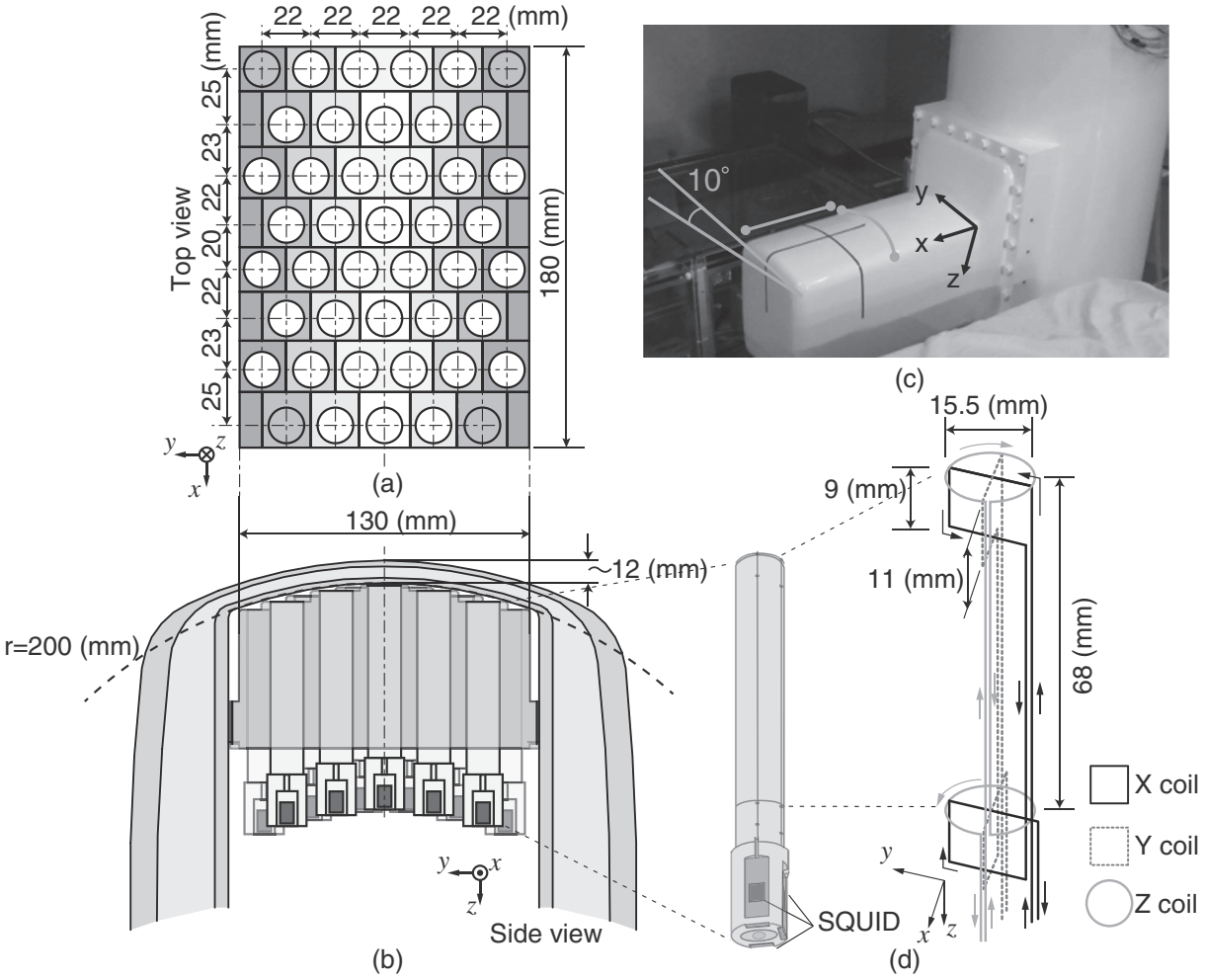

Fig. 2. Appearance and structure of the MSG system. (a) A top view and the dimensions of the array of SQUID gradiometers with a matrix-like arrangement. The four sensors in the four corners (gray circles) are axial-type gradiometers to pick up magnetic fields in the Z direction. The other 40 sensors (white circles) are vector-type SQUID gradiometers to simultaneously detect magnetic fields in three directions. (b) Side view of the sensor array and the dimensions of the cryostat. (c) Appearance of the MSG cryostat. The cryostat has a unique shape optimized for lumbar lordosis with a protrusion on the side surface of the cylindrical main body to store liquid helium. The protrusion holds the SQUID sensor array inside and has a 10° tilt. (d) Structure of the vector-type SQUID gradiometers. Each sensor is equipped with two planar-type gradiometric pickup coils and an axial-type gradiometric pickup coil combined into one bobbin. Each pickup coil is oriented perpendicularly to each other and connected to an individual SQUID to simultaneously detect the three independent components of magnetic fields. The baseline length of each gradiometric pickup coil is 68 mm and the noise level was less than 4 $fT/Hz^{0.5}$ in the white region. This figure was reproduced with permission from the report of Adachi et al. (DOI: https://doi.org//10.1109/TASC.2016.2631422). ©2017 IEEE.

the body, the Y direction was caudal to cranial, and the Z direction was from the ventral to the dorsal side of the body. All recordings were performed in a magnetically shielded room.

2.2. Subjects

The subjects were 43 healthy volunteers aged 22–64 years (mean ± SD, 42.6 ± 12.9 years), measuring 156–181 cm in height (mean ± SD, 169.2 ± 5.6 cm), and weighing 51–90 kg (mean ± SD, 65.4 ± 9.8 kg) without nervous system disease. Those over 40 years old had MRI scans of the lumbar spine and were confirmed to have no neural compression.

2.3. Recording of CEAFs and signal processing

The subject was in the supine position on a table in a magnetically shielded room with the posterior lumbar region at the cryostat of the SQUID sensor (Fig. 3). The measurement area was centered at the spinous process of L4 and placed coplanar to the lower back. For positional information, magnetic signals from marker coils on the surface of the subject's back were recorded. Lateral and frontal radiographs were taken to obtain positional information on the subject and the SQUID sensor. The peroneal nerve was electrically stimulated at the knee (square wave pulse; 5 Hz; 0.3 ms in duration) at over 1.5 times the motor nerve threshold (6.1 ± 2.0 mA in intensity). The right and left nerves were alternately stimulated and evoked magnetic fields were respectively recorded at the surface of the lower back using a 40 kHz sampling rate and 100–5000 Hz band-pass filter. Two-thousand recordings of evoked magnetic fields were averaged for each side. We adopted this number of recordings after analysis of preliminary recordings considering the data quality and subject burden. A new method of artifact reduction, dual signal subspace projection (DSSP) (Sekihara et al., 2016), was then applied to reduce artifacts from the electrical stimulation. Signal-to-noise (SN) ratios of measurements were obtained for each subject to statistically evaluate individual differences. Here, we defined the SN ratio as the ratio of the peak-to-peak amplitude values from 5 ms to 15 ms after the stimulation for the signal to the root mean square of the magnetic fields at 20–25 ms for the noise.

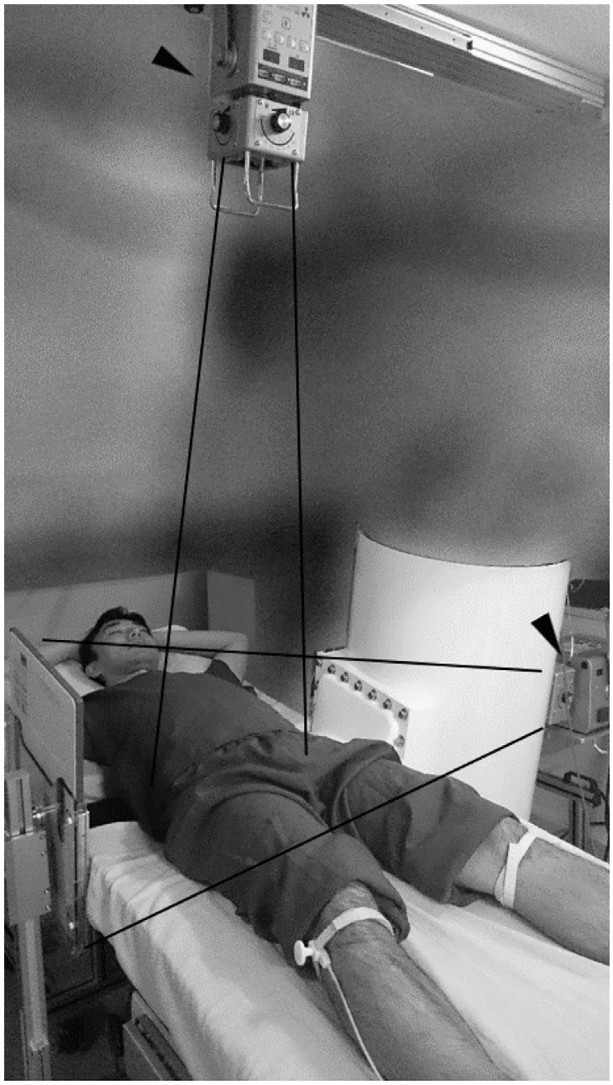

Fig. 3. The subject was in the supine position on a table in a magnetically shielded room with the posterior lumbar region on the SQUID sensor part. X-ray irradiation devices (►) were installed to take an X-ray image. Marker coils for positional information were placed under the back of the subject and the corresponding position to the lumbar spine was acquired in the anteroposterior view. In addition, a lateral X-ray image including the sensors and the lumbar spine of the subject was obtained.

Unit gain constraint recursively applied null-steering spatial filtering (UGRENS) (Kumihashi and Sekihara, 2010; Sekihara and Nagarajan, 2015) was adapted to the acquired magnetic field data to reconstruct currents induced by action potential as vector indicating the current density and direction. The reconstructed currents were superimposed on the X-ray image to visualize their distribution and intensity (Fig. 4a, b). The distance between the midpoint of the spinal canal and the surface of the sensors was used for the depth information (Fig. 4c). Through this method, the current waveforms at arbitrary points in the spinal canal and the intervertebral foramen can be calculated as if virtual electrodes were placed there.

All procedures in this study were approved by the Ethics Committee of Tokyo Medical and Dental University and carried out in accordance with the Declaration of Helsinki. We obtained written informed consent and releases for images and photographs from all participants.

Statistical analysis was performed using EZR software version 1.33 (Kanda, 2013). An unpaired two-tailed Student's *t*-test was used for single comparisons. Multiple regression analysis was used to evaluate the factors affecting the availability of CV calculation. P values of <0.05 were considered to indicate statistical significance.

2.4. Measurement of CV

Reconstructed currents perpendicularly flowing into the lumbar canal were retrieved from the virtual electrodes, which were positioned 20 mm left lateral from the midline of the lumbar canal and the presumed pathway of the spinal nerve from L3 to L5 (Fig. 4b, c). We chose this site for the calculation because previous reports from our group showed that the currents flowing into the lumbar canal are larger near the vertebral foramina contralateral to the stimulation (Ishii et al., 2012). The CVs of the reconstructed currents were calculated from the latencies of the positive peaks recorded at the virtual electrodes of L2 to L5. The average value of the left and right CVs was obtained for each subject.

3. Results

3.1. Recording of CEAFs in response to electrical stimulation of the peroneal nerve

Lumbar CEAFs were recorded in response to stimulation of the peroneal nerve at the knee from all subjects (43 subjects; 86 nerves). Fig. 5 shows isomagnetic contour maps at 9.75 ms and the evoked magnetic fields of a representative case recorded from X-, Y-, and Z-directed coils (right peroneal nerve stimulation). The peak-to-peak amplitudes were as high as 60 fT. In the contour map of X coils (Fig. 5a), positive X-directed (left to right direction) magnetic fields is depicted over the spinal canal. That of Y coils (Fig. 5b) shows that negative Y-directed (cranial to caudal) magnetic fields was mainly recorded at 9.75 ms. As shown in Fig. 5c, Z-directed coils recorded positive (ventral to dorsal directed) magnetic fields on the left side and negative magnetic fields on the right side.

In the third to fifth left column of the X coils (Fig. 5a, below), the first positive peaks (signals directed from the left to the right of the body) appeared from the caudal direction at about 10 ms after the stimulation and conducted cranially with time. The amplitude was largest at the central two columns and generally larger on the left side than on the right. In the magnetic fields from the Y coils (Fig. 5b), the negative peak (signals directed from cranial to caudal) appeared from the caudal direction around 10 ms and conducted cranially in the left four columns. At the two cranial sensors in the second right and second left columns, the polarity of the waves was reversed. In the four left columns of the magnetic fields from the Z coils (Fig. 5c), the positive waves (signals of the ventral to dorsal direction) appeared from caudal at about 8.5 ms and conducted cranially. Subsequently, the negative waves appeared at about 10–11 ms and were similarly conducted. In all three sensor coil directions, the magnetic field amplitude was generally larger on the left side.

3.2. Estimated current sources

The evoked currents reconstructed by UGRENS and converted to a pseudo-color map were superimposed on the X-ray image of the lumbar spine (Fig. 4a). Color in the map indicates current density and black arrows represent direction of reconstructed currents induced by action potentials. First, the leading component, which consisted of the currents running parallel to the nerve root, appeared from the laterocaudal area of the right side (stimulated side) and flowed into the L5/S1 intervertebral foramina (7.90 –8.60 ms, white asterisk). In all subjects, the leading components flowed into the L5/S1 foramen about 8.25–8.95 ms

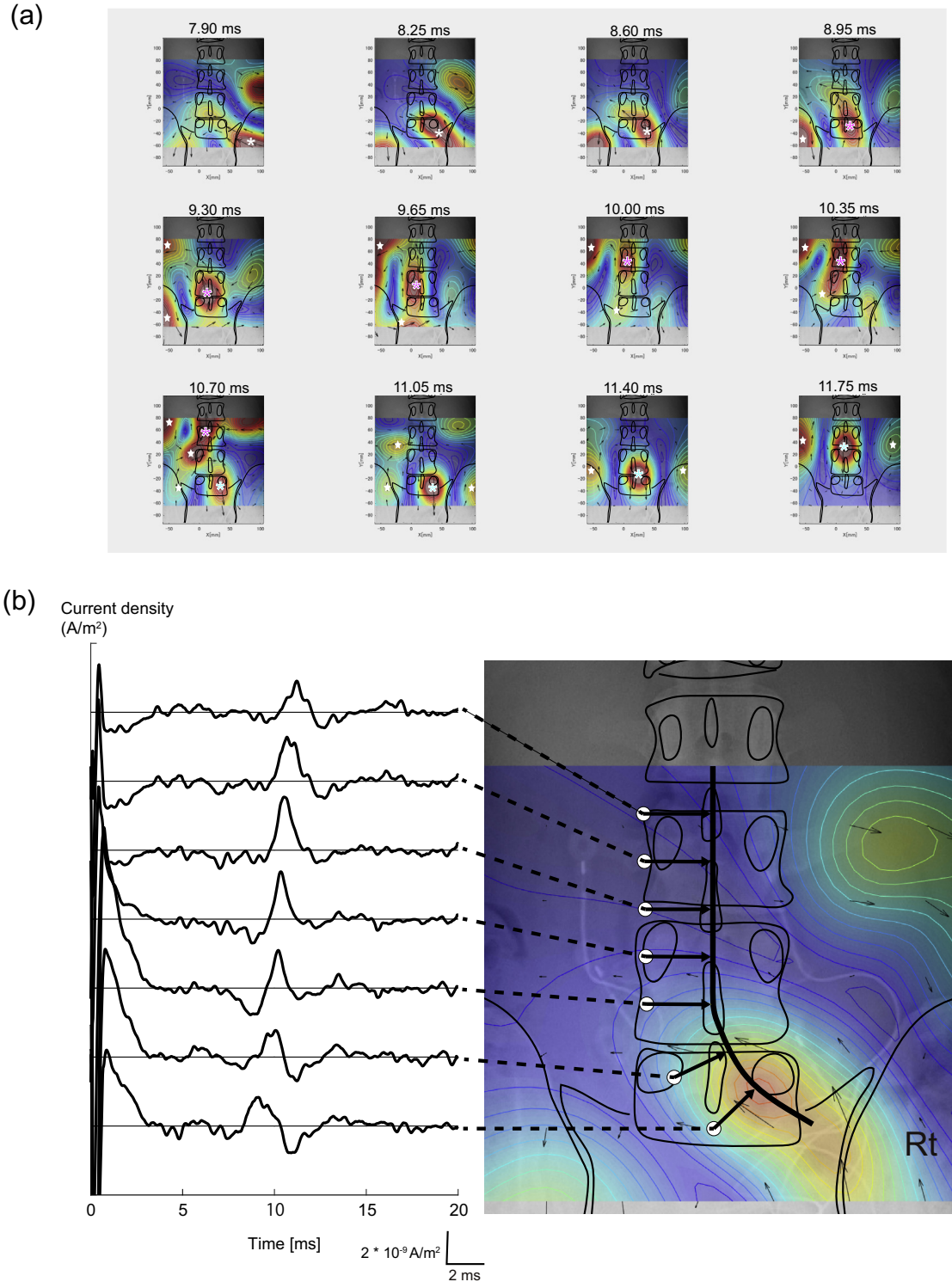

Fig. 4. (a) The evoked currents reconstructed by UGRENS are illustrated as a pseudo-color map superimposed on the X-ray image of the lumbar spine. Color indicates current density and black arrows shows direction of currents. For depth information, see (c). First, the leading components of the intra-axonal currents appeared from the stimulated side and flowed into the lumbar canal from about the right L5 foramen (7.90–8.60 ms after the stimulation, white asterisk). It propagated caudal to cranial in the spinal canal (8.95–10.00 ms, pink asterisk). Currents flowing outside of the spinal canal were recognized (8.95–10.35 ms, white stars). These currents were paralleled to the leading current, or flowing into or out of the spinal canal. Subsequently, trailing intra-axonal currents appeared (10.70–11.75 ms, light blue asterisk). Other currents flowing outside of the spinal canal appeared on the left side (10.70 ms, the lowest white star), and currents flowing in opposite direction to the trailing currents were recognized on both side of the spinal canal and propagated cranially along with the trailing current (11.05–11.75 ms, white star). (b) Virtual recording electrodes were assumed to be set 20 mm lateral from the midline of the lumbar canal. For depth information, see (c). The waveforms show reconstructed currents that were perpendicularly flowing toward the assumed conduction pathway. Upright in the waveform indicates the direction flowing perpendicularly toward the black line, which is a pathway of the spinal nerve set up to reconstruct evoked currents. The peak of the waveform conducted caudally to cranially. (c) Lateral X-ray image of the lumbar spine and the sensor. The distance between the midline of the spinal canal (yellow line) and the surface of the sensors (blue circles) was obtained for the depth information for current reconstruction. In the case of (a) and (b), the distance is about 75 mm. Blue circles overlap because several sensors are aligned.

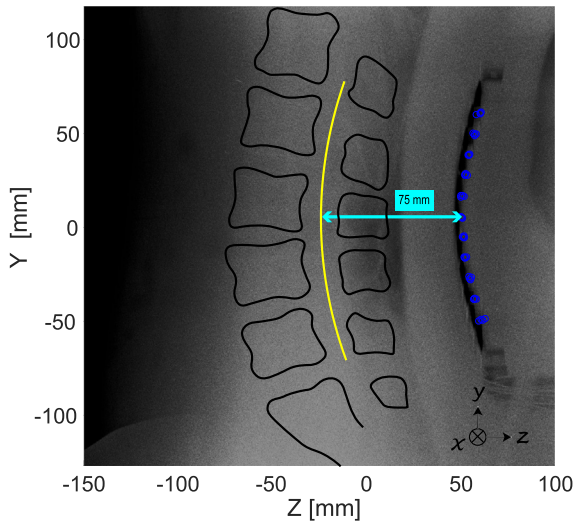

Fig. 4 (*continued*)

after the stimulation. Then, the leading currents changed their direction along the spinal canal and propagated cranially (8.95–10.0 ms, pink asterisk). In addition, currents flowing in opposite direction to the leading currents were recognized (8.95 ms, white star), and currents flowing out of and into the spinal canal were shown (9.30–10.35 ms, white stars). Subsequently, the trailing components of the intra-axonal currents appeared 10.70–11.75 ms after stimulation (light blue asterisk). Currents flowing in opposite direction to these trailing currents were depicted on the left of the nerve in 10.70 ms (the lowest white star) and on both side of the nerve from 11.05 to 11.75 ms (white stars).

3.3. CVs of the reconstructed currents in the lumbar canal

The currents perpendicularly flowing into the lumbar spine were retrieved from the virtual recording electrodes at 20 mm lateral from the midline of the lumbar canal and near the vertebral foramina (Fig. 4b). In 32 subjects (74%), the CVs of the cauda equina could be calculated from the peak latency of the volume currents at the L2–5 vertebral level where peaks were clearly identified. In the other subjects, the peaks of the waveforms were dull or the waveforms were not conductive. The subjects were categorized into two groups: those whose CVs could be calculated (Group A) and those whose CVs could not be calculated (Group B). Table 1 shows the demographic characteristics of the groups. The age and BMI were significantly higher in Group B (n = 11) than in Group A (Table 1) and the SN ratio was also significantly lower. Multiple regression analysis of the CV showed that there was a significant association with only BMI (Table 2).

In Group A, the L5, L4, L3, and L2 level latencies (mean ± SD) were 10.3 ± 0.736 ms, 10.80 ± 0.92 ms, 11.03 ± 0.59 ms, and 11.72 ± 1.45 ms, respectively. The mean CVs of the right and left side in each subject ranged from 43.8 to 85.2 m/s (n = 32; mean, 66.0 ± 9.26 m/s). A paired *t*-test showed no significant difference between the mean CVs from the right and left nerve stimulations. No subject showed marked laterality of the CV.

The distribution of the CVs in Fig. 6 showed a weak correlation between age and CV (linear regression, $y = -0.374x + 80.7$, $R^2 = 0.260$, $p < 0.005$).

4. Discussion

There have been only a few reports on evoked magnetic fields of the nervous system in the lumbar region (Mackert et al., 1997, 1998; Klein et al., 2006). Mackert et al. (1997, 1998) presented conductive magnetic fields in the lumbar area and showed that the signals of the impaired nerve disappeared in three patients with S1 nerve root compression. However, the evoked signals were small (10 fT) and the localization of the neural activities of the cauda equine or the spinal nerves was not precise enough for clinical use, mainly due to limitations in the recording device and signal processing.

Our group has reported that MSG can visualize the neural activity of the cauda equina and that the CV could be calculated from reconstructed currents in five healthy subjects (mean age, 25.4 years; CV, 56.1–66.7 m/s) (Ishii et al., 2012). However, the amplitude of the CEAFs was still small, up to 30 fT. One probable reason was that the amplitude of the CEAP after stimulation of the peripheral nerve was about one-fifth of that of the spinal cord evoked potential in response to spinal cord stimulation. Another was that the curvature of the recording area of the MSG did not fit well to the body when the flexibility of the lumbar spine was decreased due to the subject's age. When the distance between the magnetic sensors and the nerves increases, the magnetic fields recorded become smaller in a manner that is inversely proportional to the square of the distance.

In this study, we refined the shape and size of the measurement surface to decrease the distance between the lumbar region and the sensors. Stimulation at the knee could also derive larger signals because more nerve fibers can be stimulated at the proximal site and the signals attenuate or disperse to a lesser extent due to the shorter distance to the recording area. Although artifacts become larger when the stimulation is done more proximately, we could extract magnetic fields buried in artifacts using a newly developed artifact reduction method called DSSP.

When depolarization occurs in a nerve, intra-axonal currents and volume currents are generated. The site volume currents perpendicularly flowing into the nerve is considered to be the depolarization point. Considering its direction, Y sensors record volume currents flowing into and out of the nerve. Because the magnetic field is generated clockwise around the intra-axonal current, a negative magnetic field in Y coils (cranial to caudal direction) in the left side of the nerve is considered to be yielded by volume currents at the depolarization site. As Fig. 5b shows, negative magnetic fields appeared about 10 ms from the caudal site of the left four columns of the Y coils. Similarly, reconstructed currents flowing into the lumbar canal could be recognized on the left side from 9.65 ms to 11.05 ms after the stimulation (the lower white stars in 9.65–10.35 ms, the middle one in 10.70 ms and the first one on the left in 11.05 ms of Fig. 4a). We could calculate the CV of the reconstructed currents using these currents at depolarization site which are perpendicularly flowing into the spinal canal (Fig. 4b).

Ishii et al. (2012) recorded CEAPs from an epidural electrode in the lumbar canal in response to electrical stimulation of the tibial nerve in the ankle and reported that CVs calculated from the latency at L3–L5 ranged from 52.6 to 70.6 m/s (mean, 64.5 m/s). Our CVs calculated from reconstructed currents at the depolarization site ranged from 43.8 to 85.2 m/s (mean, 66.0 m/s) and are compatible with those of Ishii et al.

Taniguchi et al. (2005) used a needle electrode inserted into the ligamentum flavum and measured CEAPs in the response to tibial or peroneal nerve stimulation at the popliteal fossa. They reported that the latency of CEAPs at the L4/5 site was 10.0 ± 1.7 ms. In our study, the average latency of the reconstructed currents around L5 was 10.3 ± 0.736 ms and is thus consistent with the results of Taniguchi et al.

In this study, there was a weak correlation between age and CV (Fig. 6). It has been reported that the CV of the peripheral nerve in the limb decreases with age (Wagman and Lesse, 1952; Norris et al., 1953; Mayer, 1963; Nielsen, 1973; Taylor, 1984). Norris

et al. (1953) considered that a decrease in the CV may occur due to vascular changes in the nerve trunk. It has also been shown that the latency of SEP with posterior tibial nerve stimulation correlates with height and leg length (Lastimosa et al., 1982; Yamada et al., 1982; Tsuji et al., 1984; Chu, 1986; Kakigi, 1987).

We found significant differences between Groups A and B regarding some factors such as age, weight, and BMI (Table 1). However, there was no clear difference in height. In addition, multiple regression analysis of the CV showed that BMI was a significant factor. The SN ratios were also significantly lower in those

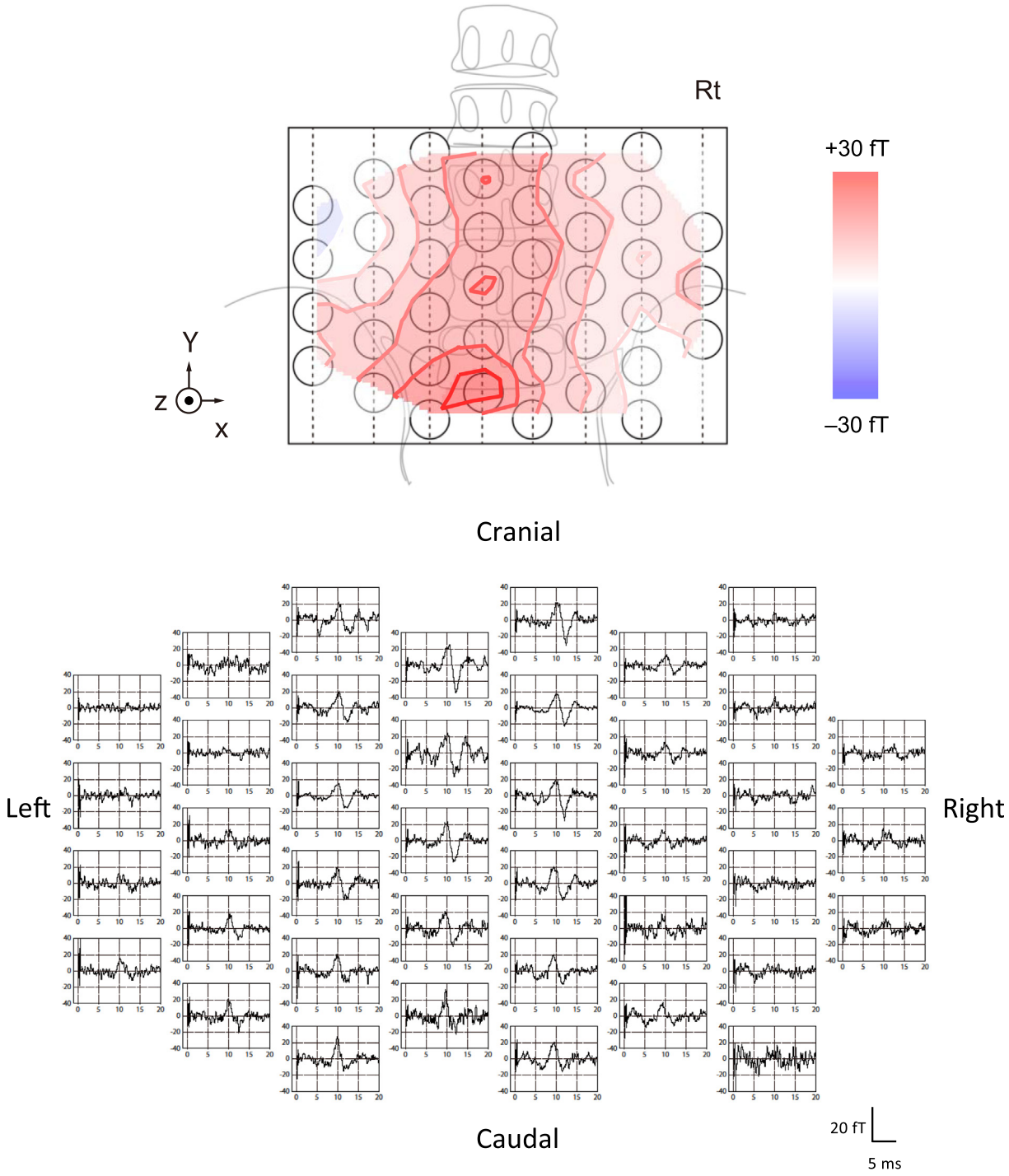

Fig. 5. Isomagnetic contour maps and waveform of magnetic fields after right peroneal nerve stimulation in a representative case. Each waveform shows magnetic fields recorded from each sensor. (a) Above is the correlation between the sensor configuration and the lumbar spine, and isomagnetic contour map of X-directed coils at 9.75 ms. Red color indicates positive X-directed magnetic fields blue means negative. Four positional sensors on the corners are not depicted; thus, there are 40 recording sensors. Below are magnetic fields recorded from X coils. The positive X direction is from the left to the right of the body. (b) Isomagnetic contour map and magnetic fields from Y coils. The positive Y direction is from caudal to cranial. (c) Isomagnetic contour map and magnetic fields from Z coils. The positive Z direction is from ventral to dorsal. Magnetic fields from the axial sensors in the four corners are depicted here.

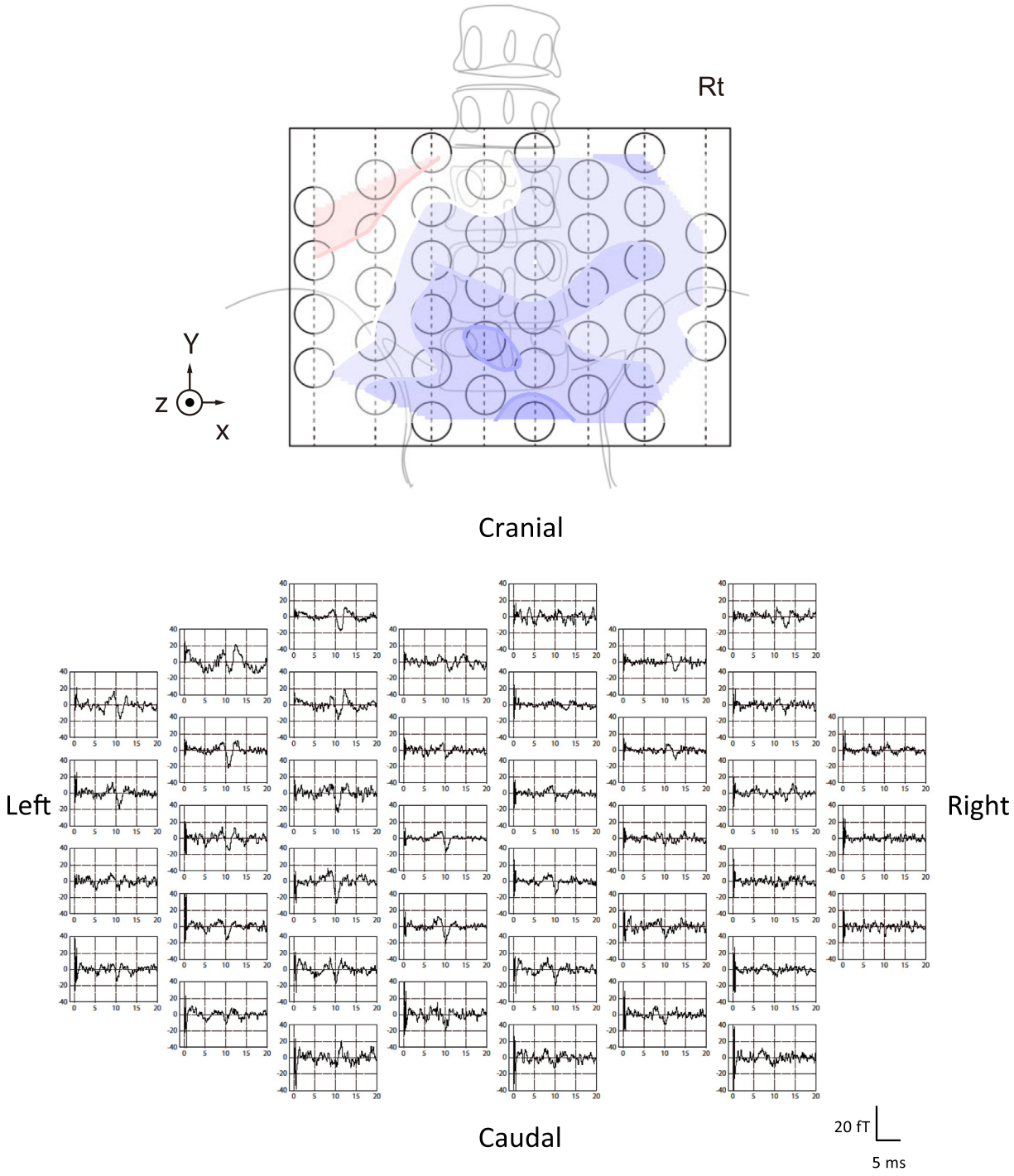

Fig. 5 (*continued*)

subjects whose CV could not be calculated (Group B). Because the magnetic field attenuated according to the distance between the sensor and signal, the negative correlation of weight and BMI to CV may be due to a larger distance between the cauda equina and the MSG sensors.

For the results of the CEAFs and reconstructed currents in response to right peroneal nerve stimulation, signals were generally larger on the left side, contralateral to the stimulus (Figs. 4a, b and 5). Considering the position of the lumbar plexus and sciatic nerve, the left side corresponds to the convex side of the conduction pathway. It could be due to the difference in the distance to the sensors, but the same phenomenon has been found in our previous studies with animal and human subjects (Tomizawa et al., 2008; Ishii et al., 2012). Although further consideration is needed, it is possible that volume currents and evoked magnetic fields are attenuated on the concave side due to signal cancellation.

One limitation of this study was the difficulty in achieving accurate recordings in patients with high BMI. As described above, the distance between the signal and recording area was larger in such cases. Further improvement of the nerve stimulation method and sensor sensitivity is necessary for accurate measurement in patients with a wider range of attributes. In addition, the method

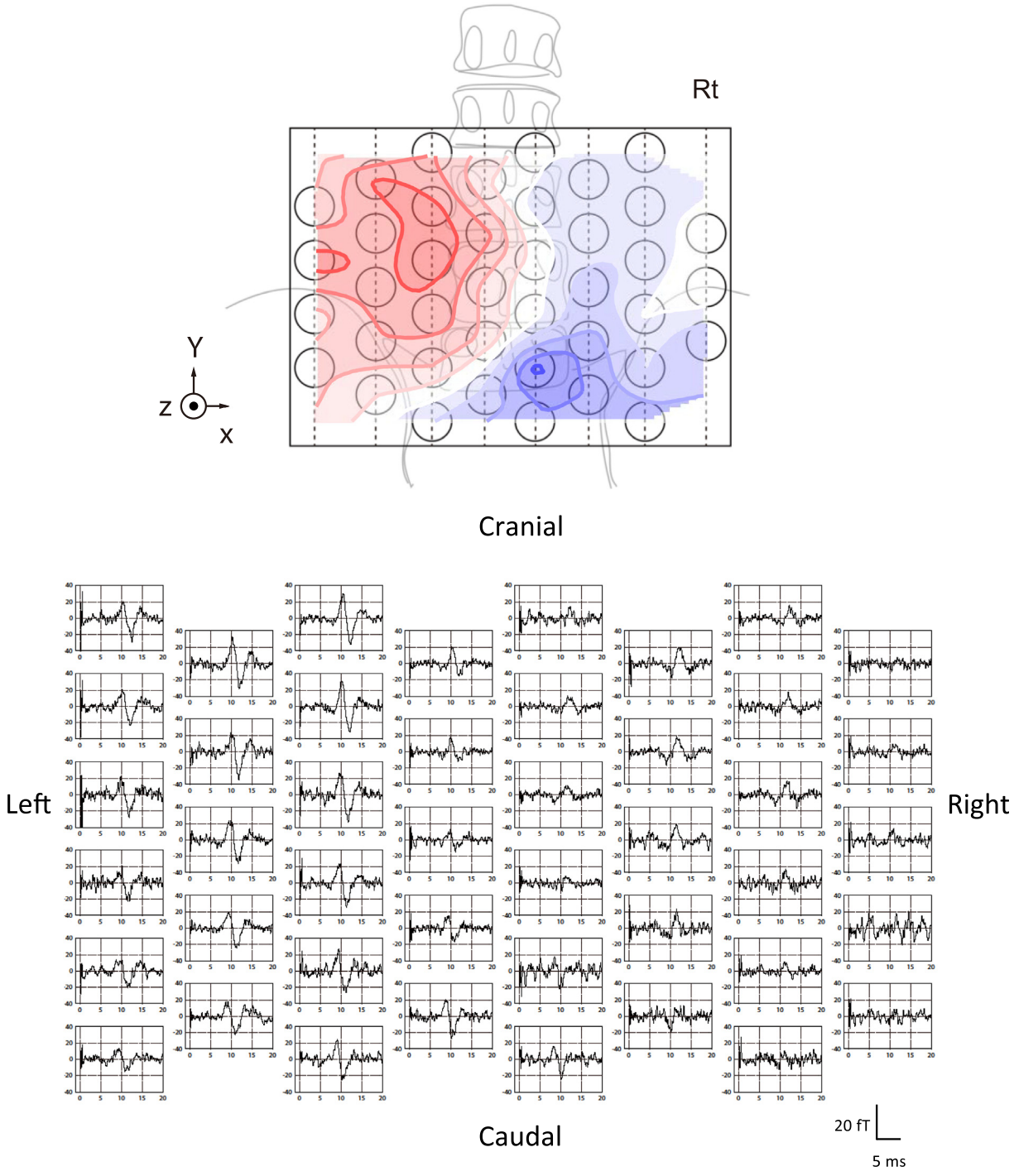

Fig. 5 (*continued*)

to evaluate each nerve in the cauda equina needs to be elucidated in the future.

It is difficult to determine the true lesion site responsible for clinical symptoms if preoperative imaging studies show multiple lesions in the spine. In practice, surgery is often performed for all suspected lesions. In the clinical setting, it is especially important to diagnose the correct lesion site in patients with L5 radiculopathy because the invasiveness of the surgical procedure differs according to whether the lesion is intra-canal or intra-foraminal. However, there is no accurate and noninvasive examination method for radiculopathy.

In this study, we showed that MSG can record CEAFs and reconstruct volume and intra-axonal currents. Notably, MSG enables observation of neural activity as currents though it is difficult by current physiological methods. Because MSG enables the evaluation of currents in the vertebral foramen and the spinal canal, it is possible to determine the site of the causative lesion more accurately. Clinical application of MSG is expected to contribute to reducing the burden of patients and to decrease healthcare cost by helping with minimally invasive surgical planning.

Table 1
Demographic characteristics of subjects.

	All	Velocity calculated group (Group A)	Velocity not calculated group (Group B)	*p* value[a]
N	43	32	11	
	Mean (SD)			
Age (years)	42.6 (12.9)	40.0 (12.9)	49.6 (10.2)	0.0218*
Height (cm)	169.4 (5.6)	169.2 (7.0)	169.8 (4.4)	0.736
Weight (kg)	63.4 (9.8)	63.1 (8.2)	71.0 (11.6)	0.0148*
BMI	22.7 (3.05)	21.9 (2.7)	24.7 (3.1)	0.0045*
Signal (fT)	42.9 (16.9)	45.9 (18.4)	36.0 (10.5)	0.0123*
SN ratio	11.4 (3.65)	12.0 (3.7)	10.0 (3.3)	0.0224*

SD, standard deviation; BMI, body mass index; fT, femtotesla.
[a] p value obtained from t-test.
* $p < 0.05$.

Table 2
Results of multivariate regression analysis.

	Regression coefficient	Standard error	t value	*p* value
BMI	−0.0531	0.0217	−2.447	0.0189*
Age	−0.00887	0.00519	−1.708	0.0955

BMI, body mass index.
* $p < 0.05$.

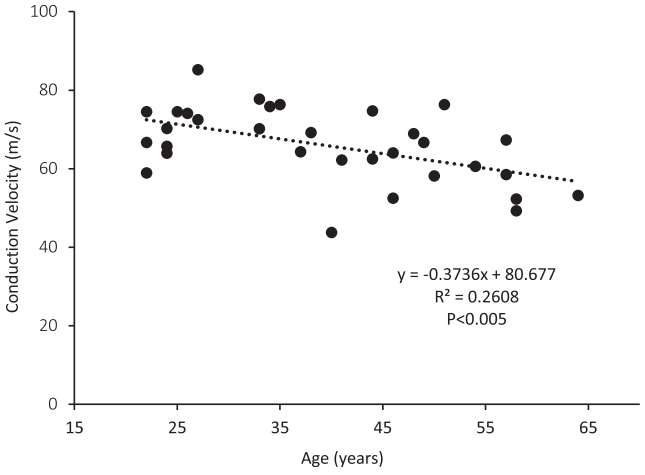

Fig. 6. Correlation between age and the conduction velocity of reconstructed currents. A weak negative correlation is evident.

5. Conclusions

This study demonstrated noninvasive visualization of the neural activity of the lumbar spinal nerve root and cauda equina after peroneal nerve stimulation at the skin surface of the knee. The data obtained from healthy volunteers in this study could help to establish criteria for the diagnosis of L5 radiculopathy by comparison with data from patients with L5 radiculopathy. Future studies using MSG will establish a diagnostic method for spinal nerve pathology and lead to minimally invasive surgery, which may reduce the burden on patients and medical expenses.

Acknowledgements

This research was supported by the RICOH Company. The funding body played no role in study design, data collection and analysis, preparation of the manuscript, or the decision to publish. The authors thank Mr. Y. Kawabata, Mr. H. Hanamoto, Miss H. Kusumi, and Miss A. Nomura of Tokyo Metropolitan University and Mr. H. Deguchi and Mr. T. Yamaga of RICOH Company for their generous help and technical assistance.

Declaration of interest

None of the authors have potential conflicts of interest to be disclosed.

References

Adachi Y, Kawai J, Miyamoto M, Ogata H, Tomori M, Kawabata S, et al. A SQUID system for measurement of spinal cord evoked field of supine subjects. IEEE Trans Appl Supercond 2009;19:861–6.
Adachi Y, Kawai J, Uehara G, Miyamoto M, Tomizawa S, Kawabata S. A 75-ch SQUID biomagnetometer system for human cervical spinal cord evoked field. IEEE Trans Appl Supercond 2007;17:3867–73.
Adachi Y, Miyamoto M, Kawai J, Uehara G, Ogata H, Kawabata S, et al. Improvement of SQUID magnetometer system for extending application of spinal cord evoked magnetic field measurement. IEEE Trans Appl Supercond 2011;21:485–8.
Adachi Y, Oyama D, Kawai J, Kawabata S, Uehara G. Spinal cord evoked magnetic field measurement using a magnetospinography system equipped with a cryocooler. Conf Proc IEEE Eng Med Biol Soc 2013;2013:4426–9.
Adachi Y, Kawabata S, Sasano T, Haruta Y, Oyama D, Uehara G, et al. Biomagnetic measurement system for supine subjects with expanded sensor array and real-time noise reduction. Conf Proc IEEE Eng Med Biol Soc 2015;2017:7071–4.
Ando M, Tamaki T, Kawakami M, Minamide A, Nakagawa Y, Maio K, et al. Electrophysiological diagnosis using sensory nerve action potential for the intraforaminal and extraforaminal L5 nerve root entrapment. Eur Spine J 2013;22:833–9.
Chu NS. Somatosensory evoked potentials: correlations with height. Electroencephalogr Clin Neurophysiol 1986;65:169–76.
Cracco RQ. Spinal evoked response: peripheral nerve stimulation in man. Electroencephalogr Clin Neurophysiol 1973;35:379–86.
Fukuoka Y, Komori H, Kawabata S, Ohkubo H, Shinomiya K. Visualization of incomplete conduction block by neuromagnetic recording. Clin Neurophysiol 2004;115:2113–22.
Fukuoka Y, Komori H, Kawabata S, Ohkubo H, Shinomiya K, Terasaki O. Imaging of neural conduction block by neuromagnetic recording. Clin Neurophysiol 2002;113:1985–92.
Hashimoto I, Odaka K, Gatayama T, Yokoyama S. Multichannel measurements of magnetic compound action fields of the median nerve in man. Electroencephalogr Clin Neurophysiol 1991;81:332–6.
Imajo Y, Kanchiku T, Suzuki H, Funaba M, Nishida N, Fujimoto K, et al. Cauda equina conduction time determined by F-waves in normal subjects and patients with neurogenic intermittent claudication caused by lumbar spinal stenosis. J Clin Neurophysiol 2017;34:132–8.
Ishii S, Kawabata S, Tomizawa S, Tomori M, Sakaki K, Shinomiya K, et al. Conductive neuromagnetic fields in the lumbar spinal canal. Clin Neurophysiol 2012;123:1656–61.
Jonsson B, Stromqvist B, Annertz M, Holtas S, Sunden G. Diagnostic lumbar nerve root block. J Spinal Disord 1988;1:232–5.
Kakigi R. The effect of aging on somatosensory evoked potentials following stimulation of the posterior tibial nerve in man. Electroencephalogr Clin Neurophysiol 1987;68:277–86.
Kakigi R, Shibasaki H, Hashizume A, Kuroiwa Y. Short latency somatosensory evoked spinal and scalp-recorded potentials following posterior tibial nerve stimulation in man. Electroencephalogr Clin Neurophysiol 1982;53:602–11.
Kanda Y. Investigation of the freely available easy-to-use software 'EZR' for medical statistics. Bone Marrow Transplant 2013;48:452–8.
Kawabata S, Komori H, Mochida K, Harunobu O, Shinomiya K. Visualization of conductive spinal cord activity using a biomagnetometer. Spine 2002;27:475–9.
Kent DL, Haynor DR, Larson EB, Deyo RA. Diagnosis of lumbar spinal stenosis in adults: a metaanalysis of the accuracy of CT, MR, and myelography. AJR Am J Roentgenol 1992;158:1135–44.

Klein A, van Leeuwen P, Hoormann J, Gronemeyer D. Magnetoneurographic registration of propagating magnetic fields in the lumbar spine after stimulation of the posterior tibial nerve. J Neural Eng 2006;3:125–31.
Kumihashi I, Sekihara K. Array-gain constraint minimum-norm spatial filter with recursively updated gram matrix for biomagnetic source imaging. IEEE Trans Biomed Eng 2010;57:1358–65.
Kunogi J, Hasue M. Diagnosis and operative treatment of intraforaminal and extraforaminal nerve root compression. Spine (Phila Pa 1976) 1991 ():1312–20.
Lastimosa AC, Bass NH, Stanback K, Norvell EE. Lumbar spinal cord and early cortical evoked potentials after tibial nerve stimulation: effects of stature on normative data. Electroencephalogr Clin Neurophysiol 1982;54:499–507.
Levin KH. L5 radiculopathy with reduced superficial peroneal sensory responses: intraspinal and extraspinal causes. Muscle Nerve 1998;21:3–7.
Mackert BM, Curio G, Burghoff M, Marx P. Mapping of tibial nerve evoked magnetic fields over the lower spine. Electroencephalogr Clin Neurophysiol 1997;104:322–7.
Mackert BM, Curio G, Burghoff M, Trahms L, Marx P. Magnetoneurographic 3D localization of conduction blocks in patients with unilateral S1 root compression. Electroencephalogr Clin Neurophysiol 1998;109:315–20.
Macnab I. Negative disc exploration. An analysis of the causes of nerve-root involvement in sixty-eight patients. J Bone Joint Surg Am 1971;53:891–903.
Mamisch N, Brumann M, Hodler J, Held U, Brunner F, Steurer J, et al. Radiologic criteria for the diagnosis of spinal stenosis: results of a Delphi survey. Radiology 2012;264:174–9.
Matsumoto H, Octaviana F, Terao Y, Hanajima R, Yugeta A, Hamada M, et al. Magnetic stimulation of the cauda equina in the spinal canal with a flat, large round coil. J Neurol Sci 2009;284:46–51.
Mayer RF. Nerve conduction studies in man. Neurology 1963;13:1021–30.
Nielsen VK. Sensory and motor nerve conduction in the median nerve in normal subjects. Acta Med Scand 1973;194:435–43.
Norris AH, Shock NW, Wagman IH. Age changes in the maximum conduction velocity of motor fibers of human ulnar nerves. J Appl Physiol 1953;5:589–93.
Ohkubo H, Komori H, Kawabata S, Fukuoka Y, Shinomiya K. Estimation of localization of neural activity in the spinal cord using a biomagnetometer. J Med Dent Sci 2003;50:177–82.
Olsewski JM, Simmons EH, Kallen FC, Mendel FC. Evidence from cadavers suggestive of entrapment of fifth lumbar spinal nerves by lumbosacral ligaments. Spine (Phila Pa 1976) 1991(16):336–47.
Secil Y, Ekinci AS, Bayram KB, Incesu TK, Tokucoglu F, Gurgor N, et al. Diagnostic value of cauda equina motor conduction time in lumbar spinal stenosis. Clin Neurophysiol 2012;123:1831–5.
Sekihara K, Nagarajan SS. Electromagnetic brain imaging: a Bayesian perspective. Basel (Switzerland): Springer International Publishing; 2015.
Sekihara K, Kawabata Y, Ushio S, Sumiya S, Kawabata S, Adachi Y, et al. Dual signal subspace projection (DSSP): a novel algorithm for removing large interference in biomagnetic measurements. J Neural Eng 2016;13:036007.
Senocak O, Hurel DM. Sener U, Ugurel B, Oztura I, Ertekin C. Motor conduction time along the cauda equina in patients with lumbar spinal stenosis. Spine (Phila Pa 1976) 2009(34):1410–4.
Sumiya S, Kawabata S, Hoshino Y, Adachi Y, Sekihara K, Tomizawa S, et al. Magnetospinography visualizes electrophysiological activity in the cervical spinal cord. Sci Rep 2017;7:2192.
Taniguchi S, Kawada T, Ushida T, Nagano Y, Ikemoto T, Tani T. Analysis of cauda equina action potentials recorded from the ligamentum flavum after peroneal nerve and tibial nerve stimulation during surgery for lumbosacral radiculopathies. Int Congr Ser 2005;1278:109–12.
Taylor PK. Non-linear effects of age on nerve conduction in adults. J Neurol Sci 1984;66:223–34.
Tomizawa S, Kawabata S, Komori H, Hoshino Fukuoka Y, Shinomiya K. Evaluation of segmental spinal cord evoked magnetic fields after sciatic nerve stimulation. Clin Neurophysiol 2008;119:1111–8.
Tomori M, Kawabata S, Tomizawa S, Ishii S, Enomoto M, Adachi Y, et al. Diagnosis of incomplete conduction block of spinal cord from skin surface using spinal cord evoked magnetic fields. J Orthop Sci 2010;15:371–80.
Trahms L, Erné SN, Trontelj Z, Curio G. Biomagnetic functional localization of a peripheral nerve in man. Biophys J 1989;55:1145–53.
Tsuji S, Luders H, Lesser RP, Dinner DS, Klem G. Subcortical and cortical somatosensory potentials evoked by posterior tibial nerve stimulation: normative values. Electroencephalogr Clin Neurophysiol 1984;59:214–28.
Wagman IH, Lesse H. Conduction velocity of ulnar nerve in human subjects of different ages and sizes. J Neurophysiol 1952;15:235–44.
Wijesinghe RS. Magnetic measurements of peripheral nerve function using a neuromagnetic current probe. Exp Biol Med (Maywood) 2010;235:159–69.
Wiltse LL, Guyer RD, Spencer CW, Glenn WV, Porter IS. Alar transverse process impingement of the L5 spinal nerve: the far-out syndrome. Spine (Phila Pa 1976) 1984(9):31–41.
Yamada T, Machida M, Kimura J. Far-field somatosensory evoked potentials after stimulation of the tibial nerve. Neurology 1982;32:1151–8.
Yeom JS, Lee JW, Park KW, Chang BS, Lee CK, Buchowski JM, et al. Value of diagnostic lumbar selective nerve root block: a prospective controlled study. AJNR Am J Neuroradiol 2008;29:1017–23.